Calculation of stopping powers for protons using single point calibration method for dual energy CT

A Sarnatskiy, A Biegun, E van der Graaf
A bachelor thesis for Physics, faculty of Mathematics and Natural Sciences,
University of Groningen

Abstract

The single point calibration method introduced by Hünemohr in 2014 is analysed in this study for DECT energies 90/150Sn kV. The composition of 38 calibration materials have been used to investigate, which predicts the relative electron number density and effective atomic number accurately. Also an optimal constant α has been determined to be 3.3. The best calibration materials have been used in calculating the relative stopping power for 81 human tissues. The calibration materials AlMgSi, Al_2O_3, Carbon, SB3, Methanol show less than 1 percent relative difference compared to the relative stopping power calculated from composition; KCl even showed less than 0.1 percent accuracy. This was a theoretical study, so an experimental one is needed to confirm these results.

Introduction

Healthcare in many developed countries has greatly improved in the last decades resulting in a longer life expectancy of the population. Due to a longer life, the risk of getting cancer increases. This lead to improvement of cancer treatment for many methods by increasing the accuracy and lowering the side effects. There are several methods to treat a tumour. Occasionally, the tumour can be removed surgically, when it is big enough. However, in order to avoid recurrence of the tumour, a part of the healthy tissue needs to be removed with the tumour. If the tumour is located near vital organs, this method is most likely averted. Alternatives are chemotherapy, immunotherapy or radiotherapy. During chemotherapy a chemical substance is injected in the patients system to damage the tumour until all of its cancer cells die. As the substance is dispersed in the system, the healthy cells are damaged too, which can cause severe side effects. Immunotherapy makes use of anti-bodies targeted at the tumour. The immune system of the patient is then directed to detect the proteins on the surface of the cancer cells and attack the cells. This method is more accurate and has less side effects than chemotherapy, but is more expensive. Most commonly used radiation in radiotherapy is X-ray radiation. X-rays dispose their energy over their whole path through the body, with the so-called Bragg peak (maximal delivered energy) near the tumour region. Also this method causes damage to healthy cells and regions near vital organs and clusters of

nerves (like the spine) are avoided. All of these methods can be lethal for weak patients and can affect body development of young patients.

In contrast to this, the radiation in proton therapy disposes less energy on their path to the cancer region and disposes all of their remaining energy locally. The intensity of how much the proton is slowed down by the tissue is called the stopping power. For protons with kinetic energy in the order of 200 MeV this stopping power is mainly due to ionisation or excitation of the molecules. The confined Bragg peak of proton radiation results in less damage on the healthy cells and more on the tumour cells. In order to hit the tumour accurately, one should know which body tissues the proton penetrates and how much the respective tissues contribute to the range of the proton. How much a tissue contributes to the range can be done by investigating the composition of the tissue. This was calculated by compiling data from previous studies and calculating the content of the tissue by element (Woodard and White 1986). The body of the patient is scanned by a X-ray computed tomography scanner (X-ray CT), which provides the necessary knowledge of the tumours location and the types of tissues in the path to the tumour by means of the rate of interaction between the X-rays and the body tissue. The CT scan shows contrast between tissues, which interact differently with the X-ray; black is no interaction and white is total absorption. From such a picture one could derive characteristics from the shades of grey for every pixel. The shade of grey is measured as a Hounsfield unit (HU).

CT-scanners can be divided into two types: single energy CT (SECT) and dual energy CT (DECT). There exist several methods to convert the Hounsfield units of the image to a stopping power for a proton beam. By using SECT, one could convert by means of a direct calibration, a stoichiometric calibration or by means of a look-up table. These methods are compared by Bas de Jong. (bron B. de Jong)

Alternatively, one could measure two CT values for different energies. The advantage of the DECT is that it creates images with more contrast, so the tissues are easily distinguished. A method for DECT is introduced by Hünemohr (Hünemohr et al 2014) In this model, a single point calibration is set by water and another materials, which composition is known precisely. This calibration in turn, can calculate the relative electron number density (rEND) with respect to water and the effective atomic number (EAN), given the two

Hounsfield units of a material or tissue from the DECT scan. These values are then fitted to calculate the mean excitation potential, which in turn is used to calculate the relative stopping power (RSP). In this study, the calibration method of Hünemohr is tested and adjusted. Firstly, the calibration method for rEND and EAN is used on 38 materials, by means of virtual Hounsfield units calculated from composition. A suitable calibration material has been chosen by comparing the rEND and EAN from calibration with the calculated ones. For the six best calibration materials a constant α was fitted (α = 3.1 in Hünemohr et al). The optimal α and seven best calibration materials have been used to fit the mean excitation potential and the predict the RSP for 81 body tissues, composition of which is derived from Woodard and White. The predicted values of RSP are compared to the calculated ones in order to conclude if the single point calibration method is precise enough and to conclude which of the used materials is best for the calibration.

Materials and method

The attenuation coefficient for x-rays μ is a measure how much the intensity of the x-ray beam is decreased. It can be expressed as the product of number of particles and their cross-section. The x-rays interacts with electrons, so:

$$\mu(Z,E) = n^e(Z) \times \sigma^e(Z,E) \quad , \tag{1}$$

where n_e is the electron number density (EAN) of elements with atomic number Z, σ^e the cross-section of electrons for energy E. The cross-section depends on the interactions one considers. In the single point calibration method by Hünemohr et al (2014), the cross-section is considered to be due to the photoelectric absorption and the Compton scattering in that material, both incoherent as coherent:

$$\mu(E) \approx \sum\nolimits_Z [n^e(Z)] \times \left(c_1 f(E) + c_2 \frac{{Z_{eff}}^{\alpha}}{E^3} \right), \tag{2}$$

where $f(E)$ a function of energy due the photoelectric effect, Z_{eff} the EAN, α is a factor characteristic for the energy spectrum and c_1 and c_2 are some constants. From this point on, the attenuation coefficient will be called linear, because the interactions in the cross-sections are linear. By making use of two energy spectra from DECT, one is able to derive the rEND (eq. (3)) and the EAN (eq. (4)):

$$\left(\frac{n_i^e}{n_w^e}\right)_j^* = a_j \cdot x_{1,i} + (1 - a_j) \cdot x_{2,i} \ , \tag{3}$$

$$\left(\frac{n_i^e}{n_w^e}\right)_j^* \cdot \left(\left(Z_{eff,i}\right)_j^*\right)^\alpha = b_j \cdot x_{1,i} + \left({Z_{eff,w}}^\alpha - b_j\right) \cdot x_{2,i} \ , \tag{4}$$

where the star (*) indicates that the value is calculated by the calibration. a_j and b_j are the calibration constant, the index *j* refers to the material, which was used to obtain the calibration constants, and $x_{1,i}$ and $x_{2,i}$ are the normalised Hounsfield units:

$$x_{U,i} = \frac{\bar{\mu}_{U,i}}{\bar{\mu}_{U,w}} = \frac{H_{U,i}}{1000\ HU} + 1 \quad . \tag{5}$$

For *U=1* the highest voltage (150Sn kV) was assigned to the Hounsfield unit $H_{1,i}$ and $\bar{\mu}_{1,i}$ and the lowest voltage (90 kV) to $H_{2,i}$ and $\bar{\mu}_{2,i}$. This model depends on two materials: water and a calibration material. If the END and EAN are known for both materials, one could calibrate a_j and b_j by rewriting eq. (3) and (4):

$$a_j = \frac{\frac{n_j^e}{n_w^e} - x_{2,j}}{x_{1,j} - x_{2,j}} \quad \text{and} \quad b_j = \frac{\frac{n_j^e}{n_w^e} \cdot \left(Z_{eff,j}\right)^\alpha - \left(Z_{eff,w}\right)^\alpha \cdot x_{2,j}}{x_{1,j} - x_{2,j}}. \tag{6),(7}$$

In this study the normalised Hounsfield units are not measured. Instead, the effective linear attenuation coefficient is calculated in order to calculate the normalised Hounsfield units in eq. (5). The term effective is used, because the linear attenuation coefficient is dependent on energy and atomic number. (Schneider et al 2000) One should integrate the linear attenuation coefficient over the whole spectrum and all the atomic numbers to calculate the effective one:

$$\bar{\mu}_{U,i} = \frac{N_A \rho_i}{M_u} \sum_E \left[S_U(E) \sum_Z \left[\frac{\omega_i(Z) \sigma^a(E,Z)}{A(Z)} \right] \right] , \tag{8}$$

where

$\bar{\mu}_{U,i}$	: effective linear attenuation coefficient of material *i* integrated over the spectrum and atomic numbers
N_A	: number of Avogadro
M_u	: conversion factor 1 gram per mole
A(Z)	: atomic weight of element Z

ρ_i : mass density of material *i*

ω_i : atomic composition of material *i*

$\sigma^a(E,Z)$: atomic cross-section spectrum (Hubell and Seltzer 1989)

$S_U(E)$: Siemens DECT energy spectrum for voltage U (Abbema 2016)

In the derivation of eq. (8), the Bragg's additivity rule has been applied by multiplying the cross-section of electrons with the number of electrons present in the atom:

$$Z \cdot \sigma^e = \sigma^a \tag{9}$$

Along with the effective linear attenuation coefficient, also the EAN and END have been calculated by composition:

$$\left(Z_{eff,i}\right)^\alpha = \frac{\sum_Z \tilde{n}_i^e(Z) \cdot Z^\alpha}{\sum_Z \tilde{n}_i^e(Z) \cdot Z} \tag{10}$$

$$n_i^e = \frac{N_A \rho_i}{M_u} \cdot \sum_Z \left[\frac{\omega_i(Z) \cdot Z}{A(Z)}\right], \tag{11}$$

where $\tilde{n}_i^e(Z)$ accounts for the electron number density of material *i* contributed by element Z and n_i^e accounts for the electron number density for all elements:

$$n_i^e = \sum_Z \tilde{n}_i^e(Z)\,. \tag{12}$$

These values are used as comparison for the values from the calibrated model. From such comparison one could conclude how well this model predicts the rEND and EAN. This comparison is calculated by variance:

$$Var(\chi, j) = \frac{1}{N-1} \sum_{i=1}^{N} \left[(\chi_i)_j^* - \chi_i\right]^2, \tag{13}$$

where N is the total number of materials and $(\chi_i)_j^*$ is either rEND or EAN of material *i* based on material *j*. The best calibration material should have the lowest variance. Besides the optimal material, this variance was used to find the optimal value for α. According to Hünemohr et al, the constant α is equal to 3.1 . This constant was varied for some materials from 1 to 5 in steps of 0.1 and from 3.1 to 3.5 in steps of 0.01, to find a minimum for the variance. The best calibration material and constant α was then used in further calculations for human tissues.

The stopping power of a charged particle by an material *i* is described by the Bethe's formula (Martin 2009):

$$-\langle\frac{dE}{dx}\rangle_i = \frac{n_i^e z^2 {q_e}^4}{4\pi{\epsilon_0}^2 m_e c^2 \beta^2}\left(\ln\left(\frac{2m_e c^2\beta^2}{I_i(1-\beta^2)}\right)-\beta^2\right), \quad (14)$$

where

$-\langle\frac{dE}{dx}\rangle$	: energy loss over an infinitesimal distance
q_e	: electron charge in Coulomb
ϵ_0	: vacuum permittivity
m_e	: electron mass
c	: speed of light
β	: speed of the particle relative to light
I	: mean excitation potential
z	: charge of the incoming particle in multiples of q_e

For this study an incoming beam of protons is considered. Given a kinetic energy of the proton *T* and its mass m_p, β is calculated by:

$$\beta^2 = 1-\left(1+\frac{T}{m_p c^2}\right)^{-2}. \quad (15)$$

By dividing the stopping power for material *i* by the one for water, most of the constants are eliminated and the RSP is calculated:

$$RSP_i = \frac{-\langle\frac{dE}{dx}\rangle_i}{-\langle\frac{dE}{dx}\rangle_w} = \frac{n_i^e}{n_w^e}\cdot\frac{\ln\left(\frac{2m_e c^2\beta^2}{1-\beta^2}\right)-\beta^2-\ln I_i}{\ln\left(\frac{2m_e c^2\beta^2}{1-\beta^2}\right)-\beta^2-\ln I_w}. \quad (16)$$

The mean excitation potential I_i is calculated by (Yang 2010):

$$\ln I_i = \frac{\sum_Z\left[\frac{\omega_i(Z)\cdot Z}{A(Z)}\cdot\ln I(Z)\right]}{\sum_Z\frac{\omega_i(Z)\cdot Z}{A(Z)}} \quad (17)$$

where the excitation potential $I(Z)$ for a given element Z is taken from (Seltzer and Berger 1982). After calculating the calibrated values of EAN, a linear fit is made between $ln\, I_i$ and $\left(Z_{eff,i}\right)_j^*$:

$$\ln I_i = c \cdot \left(Z_{eff,i}\right)_j^* + d \tag{18}$$

$\ln {I_{i,j}}^*$ are the values on the fitted line in eq. (18) at point $\left(Z_{eff,i}\right)_j^*$. By using the $\ln I^*$ from the fit and the $\left(\frac{n_i^e}{n_w^e}\right)^*$ from the calibration, the RSP^{**} can be calculated:

$${RSP_{i,j}}^{**} = \frac{-\langle\frac{dE}{dx}\rangle_{i,j}}{-\langle\frac{dE}{dx}\rangle_w} = \left(\frac{n_i^e}{n_w^e}\right)_j^* \cdot \frac{\ln\left(\frac{2m_e c^2\beta^2}{1-\beta^2}\right) - \beta^2 - \ln {I_{i,j}}^*}{\ln\left(\frac{2m_e c^2\beta^2}{1-\beta^2}\right) - \beta^2 - \ln I_w}, \tag{19}$$

As a last comparison, the fitted and calibrated value of RSP^{**} is compared to RSP, which is calculated solely from the composition:

$$\Delta_{rel} = \frac{SPR_{i,j}^{w\,**} - SPR_i^w}{SPR_i^w} \times 100\% \tag{20}$$

This is, just as the variance in eq. (13), a measure how well the model approximates.

Results

First, the optimal calibration material and the optimal α has been determined by eq. (13) for 38 materials. The values calculated from the composition by eq. (5), (8), (11) and (11) are listed in appendix A Table 2. By using the calculated rEND and EAN, the calibration parameters *a* and *b* have been determined for every material with eq. (6),(7). These parameters are also listed in Table 2. Note that for some materials, which have similar composition, the *a* and *b* parameters are equal to one and another up to some decimal. By using the calibration parameters of one material, the EAN* and rEND* have been calculated for all the other materials with eq. (3) and (4). The variance of all 38 materials between the values calculated from composition and from calibration are plotted in Figure 4. The 7 best calibration materials are plotted in Figure 1. Note that materials with aluminium provide the least variance. Since the rEND is explicitly present in the calculation of RSP (eq. (16)), one would expect that the material with the

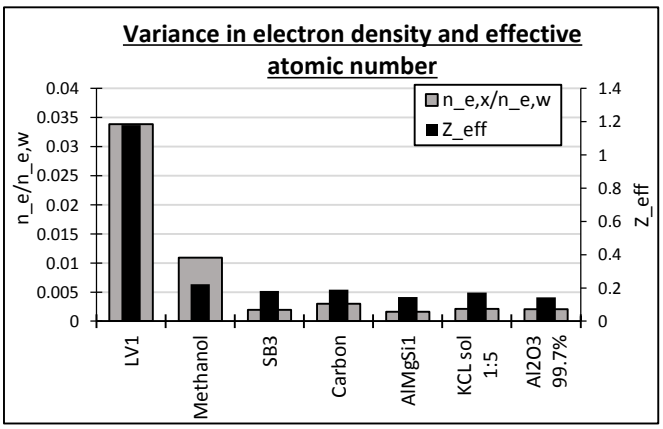

Figure 1, Variance of rEND and EAN for 7 best calibration materials

least variance in rEND, will show a low relative difference in RSP.

Secondly, the optimal α has been determined. Since variations of α only affects EAN (eq. (4)), only the variation of EAN is relevant for the investigation of the optimal α. The 7 best calibration materials were used to find the optimal α. The resulting plot is shown in Figure 2. It is evident that for the energy spectra of this study (90kV and 150kVSN) the optimal α is different from 3.1, instead, the optimal α is close to 3.3 .

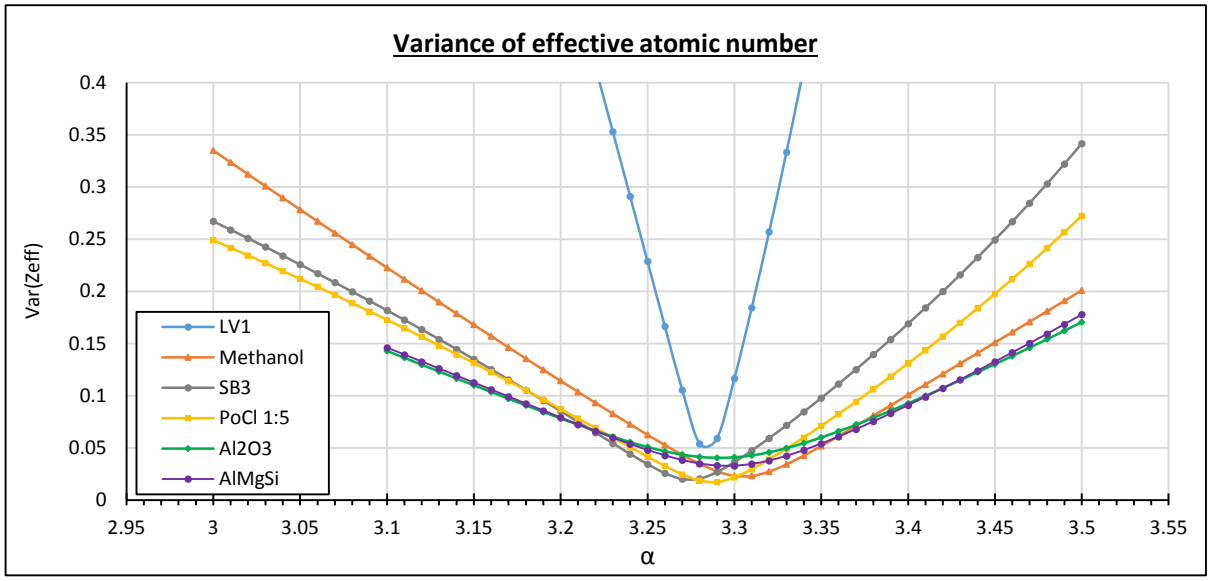

Figure 2, Variance of EAN plotted for different α's for 7 best materials

Lastly, the 7 best calibration materials and the optimal α were used to calculate the RSP for another set of 81 human tissues. The calculated values from the composition are tabulated in Appendix B Table 3. The values were used to calculate RSP according to eq. (16). In order to calculate RSP*, the linear fit of eq. (18) was performed with the calibrated values of EAN for the 81 human tissues. All of the 7 calibration materials have shown similar fits. One of them is plotted in Figure 3. From the fitted linear function, the fitted value of ln(I)* is calculated and along with rEND* the RSP** is determined according to eq. (19). The relative differences of RSP** calibrated by KCl and AlMgSi, which were calculated with eq. (20), are plotted in Figure 5 and Figure *6*. The averages of the relative differences of RSP** for the 7 calibration materials have been tabulated in Table 1.

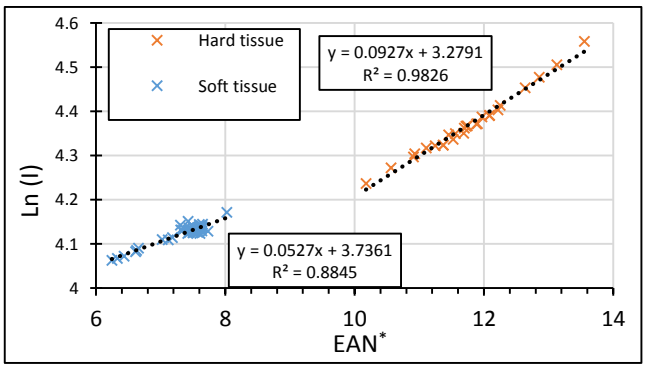

Figure 3, linear fit of *ln(I)* vs. EAN*, calibrated by AlMgSi

Materials	Average relative difference (%)
KCl 1:5	0.095
AlMgSi	0.132
Al2O3	0.160
Carbon	0.197
SB3	0.457
Methanol	0.457
LV1	1.112

Table 1, average relative difference

Discussion

There are several points that need to be pointed out. Firstly, when investigating the optimal α, some of the $EAN^{**\alpha}$ were calculated to be negative by eq. (4). This indicates that the model fails, when α is chosen higher than 3.7 .

Secondly, after getting the result of the best calibration materials in Figure 4, it was hypothesised that the material with lowest variance in rEND, will show the lowest relative difference in RSP. Both AlMgSi and Al_2O_3 have an average variance lower than the average variance of KCl, but still KCl manages to approximate the RSP closer than the aluminium-like materials. Either this is a beneficial result of the fitted $ln(I)^*$ or there is a balance of low variance in rEND and EAN, which result in low relative difference in RSP.

Lastly, an experimental study is needed to confirm these results. This can be done by gathering some, if not all, of the calibration materials and scan them with DECT. After the scan, one could calibrate the model and predict the RSP. After radiating the materials and measuring how much the proton beam has been attenuated by the materials, one could compare these results with the prediction. This would indicate better whether the model is applicable.

Conclusion

The single point calibration method introduced by Hünemohr et al (2014) shows promising results. For KCl, AlMgSi, Al_2O_3, Carbon, SB3 and Methanol as calibration materials the accuracy of RSP was less than one percent, compared to theoretical values calculated

from composition. KCl showed the best accuracy. This model is needs little time to calculate the RSP, after a proper calibration and fitting has been done.

Furthermore, a proper α has been found for the selected energies of the DECT scanners (90 kV and 150Sn kV). For these energies, the optimal α was determined to be equal to 3.3 . This α is significantly different, compared to the α defined by Hünemohr et al (2014), which was equal to 3.1 for energies 80/140Sn kV and 100/140Sn kV.

Finally, the results should be tested experimentally to confirm the precision. This can be done by collecting the materials used in this study and scan them with DECT with the energies 90 kV and 150Sn kV. After calibrating and fitting, one could predict the stopping power for selected materials and test the prediction by measuring how much a proton beam is attenuated by the material.

References

- Hünemohr N, Krauss B, Tremmel C, Ackermann B, Jäkel O, Greilich S 2014 Experimental verification of ion stopping power prediction from dual energy CT data in tissue surrogates *Phys. Med. Biol.* **59 p.**83-96
- Woodard H Q, White D T 1986 The composition of body tissues *Br. J. Radiol.* **59** p.1209-1218
- Schneider W, Brotfeld T, Schlegel W 2000 Correlation between CT numbers and tissue parameters needed for Monte Carlo simulations of clinical dose distributions *Phy. Med. Biol.* **45** p.459-478
- Hubell J H, Seltzer S M 1989 Tables of x-ray mass attenuation coefficients and mass energy-absorption coefficients from 1 keV to 20 MeV for elements Z = 1 to 92 and 48 additional substances of dosimetric interest *Rad. Phy. Div. NIST* http://www.nist.gov/pml/data/xraycoef/index.cfm
- Abbema van J K 2016 personal communication
- Martin B R 2009 Nuclear and Particle Physics 2nd ed. *John Wiley and sons Ltd, United Kingdom* ISBN 978-0-470-74274-7 p.122
- Yang M, Virshup G, Clayton J, Zhu X R, Mohan R, Dong L 2010 Theoretical variance analysis of single- and dual-energy computed tomography methods for calculating proton stopping power ratios of biological tissues *Phy. Med. Biol.* **55** p.1343-1362
- Seltzer S M, Berger M J 1982 Evaluation of the collision stopping power of elements and compounds for electrons and positions *Int. J. Appl. Radiat. Isotopes* **33** p.1189-1218

Appendices

Appendix A

Material	EAN	rEND	x_1	x_2	a	b
water	7.445329	1	1	1	-	-
LN300	7.486112	0.282445	0.282816	0.284686	1.198197	-696.602
LN450	7.458172	0.416889	0.41723	0.419328	1.162614	49.57052
AP6	6.171128	0.92749	0.910892	0.860743	1.330977	-3444.61
BR12	6.807183	0.957719	0.948818	0.923474	1.351214	-3942.07
CT SW	7.544898	0.984628	0.987615	1.000568	1.230579	-991.474
SW M457	7.544893	1.01501	1.018087	1.031438	1.230481	-991.626
AlMgSi1	13.20714	2.336114	2.82184	4.378498	1.312032	-3056.19
BRN-SR2	6.049987	1.046947	1.026661	0.965795	1.333283	-3444.51
LV1	7.545681	1.063867	1.067103	1.081141	1.230584	-999.45
IB3	10.22391	1.105933	1.18719	1.453588	1.305019	-2845.05
B200	10.22932	1.111483	1.193357	1.461753	1.305049	-2845.6
CB2-30%	10.60644	1.275856	1.387716	1.753503	1.305807	-2852.01
CB2-50%	12.26066	1.470037	1.707162	2.477843	1.307683	-2895
SB3	13.38418	1.696019	2.077362	3.314415	1.308267	-2909.02
n-Pentane	5.385535	0.656485	0.63926	0.58841	1.338739	-3451.1
n-Hexan	5.399321	0.688815	0.670838	0.617716	1.338398	-3450.23
n-Heptane	5.409258	0.712201	0.693687	0.638935	1.338149	-3449.6
Methanol	6.71619	0.80051	0.791488	0.764679	1.336556	-3445.54
Ethanol	6.385735	0.80118	0.788677	0.751526	1.336556	-3445.54
Propan-1-ol	6.195197	0.820483	0.805795	0.762154	1.336556	-3445.54
Propan-2-ol	6.195197	0.800098	0.785775	0.743218	1.336556	-3445.54
Oleic acid	5.864057	0.898864	0.879583	0.821935	1.334454	-3440.2
Ethyl acetoacetate	6.611887	0.994173	0.981861	0.944079	1.32588	-3418.38
Polyethylene glycol	6.552247	1.102182	1.087571	1.043187	1.329209	-3426.85
Glycerol	6.884567	1.232383	1.221699	1.188915	1.325879	-3418.38
Silicon oil Siluron	10.47613	0.942615	1.01798	1.263793	1.306595	-2982.72
KCl sol 1:5	8.515869	1.015676	1.038305	1.111866	1.307636	-2938.67
KCl sol 1:2	9.308166	1.035512	1.080093	1.225007	1.307635	-2938.67
KCl sol 1:1	9.938511	1.054505	1.120372	1.33448	1.307635	-2938.67
KCl sol	11.29228	1.109318	1.2355	1.645666	1.307635	-2938.66
Carbon	6	1.526286	1.496958	1.404451	1.31703	-3395.87
UHMWPE	5.470514	0.948353	0.924302	0.852841	1.336556	-3445.54
Polypropylene	5.470514	0.944243	0.920296	0.849145	1.336556	-3445.54
Nylon 6.6-101	6.147487	1.127213	1.10664	1.04446	1.330875	-3423.58
PMMA	6.495638	1.149499	1.133499	1.084612	1.327281	-3421.94
Polycarbonaat	6.283312	1.131615	1.113078	1.055864	1.32398	-3413.55
Teflon	8.445669	1.906419	1.946076	2.0623	1.341209	-3280.24
Al2O3 99.7%	11.18014	3.438329	3.805746	4.975231	1.314171	-3084.31

Table 2, List of 38 materials with the respective EAN, rEND, normalised Hounsfield units and a,b calibration parameters for $\alpha = 3.1$

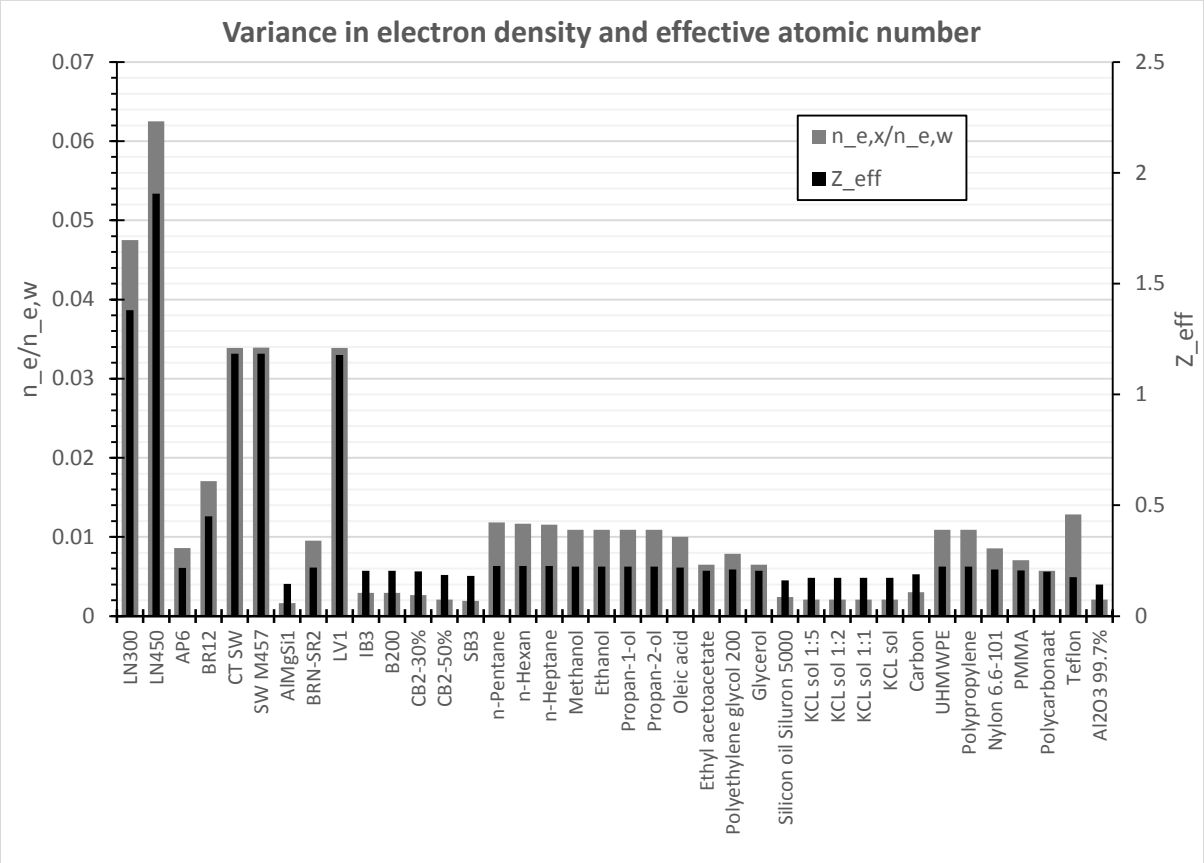

Figure 4, Variance of rEND and EAN for every material for $\alpha = 3.1$

Appendix B

Sample	Sample no.	x_1	x_2	rEND	EAN	ln(I)
water	0	1.0000	1.0000	1.0000	7.4775	4.1164
Lung - parenchyma	1	1.0430	1.0502	1.0413	7.6054	4.1367
Lung - blood filled	2	1.0429	1.0496	1.0413	7.5975	4.1363
Lung - inflated	3	0.2582	0.2599	0.2578	7.5975	4.1363
Adipose tissue 3	4	0.9157	0.8658	0.9328	6.2264	4.0619
Adipose tissue 2	5	0.9360	0.8916	0.9512	6.4210	4.0719
Adipose tissue 1	6	0.9563	0.9176	0.9696	6.5981	4.0818
Mamary gland 1	7	0.9740	0.9365	0.9869	6.6470	4.0897
Mamary gland 2	8	1.0063	0.9837	1.0143	7.0180	4.1090
Mamary gland 3	9	1.0474	1.0397	1.0504	7.3312	4.1302
Breasts	10	0.9557	0.9176	0.9687	6.6154	4.0845
Brain - cerebrospinal fluid	11	1.0107	1.0179	1.0088	7.6095	4.1233
Brain - grey matter	12	1.0373	1.0463	1.0350	7.6399	4.1288
Brain - white matter	13	1.0337	1.0352	1.0340	7.5039	4.1247
Brain and spinal cord	14	1.0360	1.0416	1.0349	7.5775	4.1258
Adrenal gland	15	1.0186	1.0034	1.0242	7.1786	4.1135
Misc. Glands	16	1.0438	1.0471	1.0432	7.5379	4.1303
Small intestine (wall)	17	1.0232	1.0214	1.0243	7.4430	4.1251
Stomach	18	1.0412	1.0395	1.0423	7.4443	4.1286
Gas.intest. tract - contents	19	1.0185	1.0203	1.0187	7.5105	4.1362
Heart 1	20	1.0406	1.0406	1.0413	7.4759	4.1304
Heart 2	21	1.0426	1.0454	1.0422	7.5294	4.1306
Heart 3	22	1.0436	1.0497	1.0423	7.5865	4.1332
Heart - blood filled	23	1.0534	1.0621	1.0512	7.6396	4.1344
Kidney 1	24	1.0404	1.0424	1.0403	7.5151	4.1342
Kidney 2	25	1.0421	1.0465	1.0413	7.5575	4.1339
Kidney 3	26	1.0438	1.0503	1.0423	7.5953	4.1335
Liver 1	27	1.0419	1.0461	1.0412	7.5532	4.1337
Liver 2	28	1.0515	1.0573	1.0502	7.5812	4.1371
Liver 3	29	1.0609	1.0680	1.0592	7.6029	4.1402
Muscle - skeletal 1	30	1.0396	1.0421	1.0394	7.5230	4.1359
Muscle - skeletal 2	31	1.0413	1.0460	1.0404	7.5635	4.1356
Muscle - skeletal 3	32	1.0423	1.0499	1.0404	7.6143	4.1379
Pancreas	33	1.0326	1.0295	1.0341	7.4204	4.1232
Ovary	34	1.0442	1.0491	1.0432	7.5647	4.1314
Prostate	35	1.0333	1.0345	1.0334	7.4996	4.1296
Testis	36	1.0347	1.0380	1.0342	7.5376	4.1281
Urine	37	1.0219	1.0363	1.0178	7.7374	4.1278
Urinary bladder - empty	38	1.0352	1.0433	1.0332	7.6239	4.1325
Gallbladder - bile	39	1.0265	1.0291	1.0261	7.5248	4.1257
Spleen	40	1.0526	1.0588	1.0512	7.5881	4.1353
Thyroid	41	1.0404	1.0388	1.0414	7.4481	4.1296
Trachea	42	1.0514	1.0600	1.0493	7.6304	4.1403

Aorta	43	1.0400	1.0496	1.0376	7.6509	4.1440
Blood - whole	44	1.0529	1.0627	1.0503	7.6597	4.1375
Blood vessels	45	1.0392	1.0461	1.0376	7.6028	4.1433
Connective tissue	46	1.1000	1.0970	1.1016	7.4209	4.1504
Eyes	47	1.0153	1.0164	1.0154	7.4974	4.1251
Eye lens	48	1.0511	1.0419	1.0546	7.3025	4.1417
Lymph	49	1.0232	1.0280	1.0221	7.5643	4.1268
Skin 1	50	1.0743	1.0652	1.0780	7.3083	4.1313
Skin 2	51	1.0754	1.0692	1.0780	7.3643	4.1340
Skin 3	52	1.0778	1.0757	1.0790	7.4387	4.1351
Skeleton - cartilage	53	1.0934	1.1272	1.0834	8.0214	4.1709
Skeleton - cortical bone	54	2.1814	3.4820	1.7806	13.6302	4.5575
Skeleton - red marrow	55	1.0163	0.9979	1.0231	7.1206	4.1082
Skeleton - spongiosa	56	1.2236	1.4663	1.1499	10.2286	4.2364
Skeleton - yellow marrow	57	0.9651	0.9154	0.9821	6.3117	4.0665
Head cranium	58	1.7764	2.6197	1.5170	12.7101	4.4526
Head mandible	59	1.8655	2.8036	1.5768	12.9295	4.4770
C4 excl. cartilage (male)	60	1.5259	2.0822	1.3551	11.8064	4.3664
D6,L3 excl. cartilage (male)	61	1.4111	1.8456	1.2779	11.3078	4.3218
C4 incl. cartilage (male)	62	1.4704	1.9578	1.3209	11.5160	4.3460
D6,L3 incl. cartilage (male)	63	1.3673	1.7415	1.2527	10.9839	4.3035
Vertebral column whole (male)	64	1.4053	1.8170	1.2791	11.1655	4.3167
Sternum	65	1.3042	1.6118	1.2103	10.6166	4.2713
Clavicle, scapula	66	1.5865	2.2299	1.3890	12.1526	4.3902
Ribs 2nd, 6th (male)	67	1.5136	2.0569	1.3469	11.7579	4.3613
Ribs 10th (male)	68	1.6575	2.3633	1.4406	12.3185	4.4130
Humerus (total bone)	69	1.5864	2.2297	1.3890	12.1521	4.3901
Humerus spherical head	70	1.4186	1.8754	1.2789	11.4327	4.3231
Humerus cylindrical shaft	71	1.6251	2.3099	1.4148	12.2833	4.4031
Humerus whole specimen	72	1.4954	2.0309	1.3314	11.7507	4.3498
Pelvic innominate (male)	73	1.5140	2.0626	1.3456	11.7875	4.3655
Pelvic innominate (female)	74	1.5791	2.1974	1.3892	12.0355	4.3866
Pelvic sacrum (male)	75	1.3571	1.7260	1.2443	10.9695	4.2961
Pelvic sacrum (female)	76	1.4868	1.9971	1.3303	11.6202	4.3494
Femur (total bone)	77	1.5342	2.1189	1.3549	11.9480	4.3709
Femur sperical head	78	1.4186	1.8754	1.2789	11.4327	4.3231
Femur conical trochanter	79	1.4563	1.9500	1.3052	11.5841	4.3360
Femur cylindrical shaft	80	1.9611	3.0178	1.6359	13.2033	4.5052
Femur whole specimen	81	1.5462	2.1389	1.3645	11.9668	4.3718

Table 3, calculated normalised Hounsfield units, rEND, EAN and *ln(I)* for 81 human tissues

Appendix C

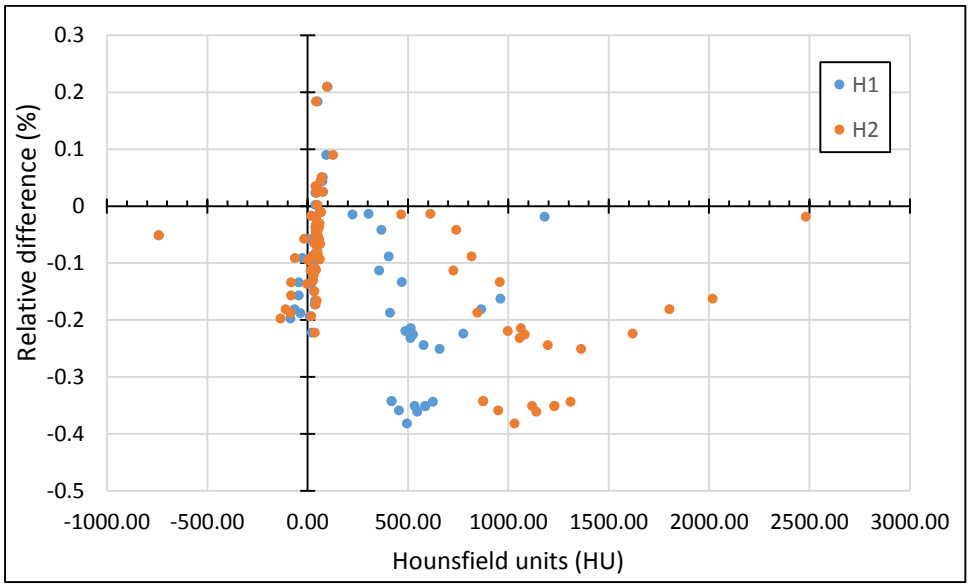

Figure 5, relative difference of RSP** vs. Hounsfield units, calibrated by AlMgSi

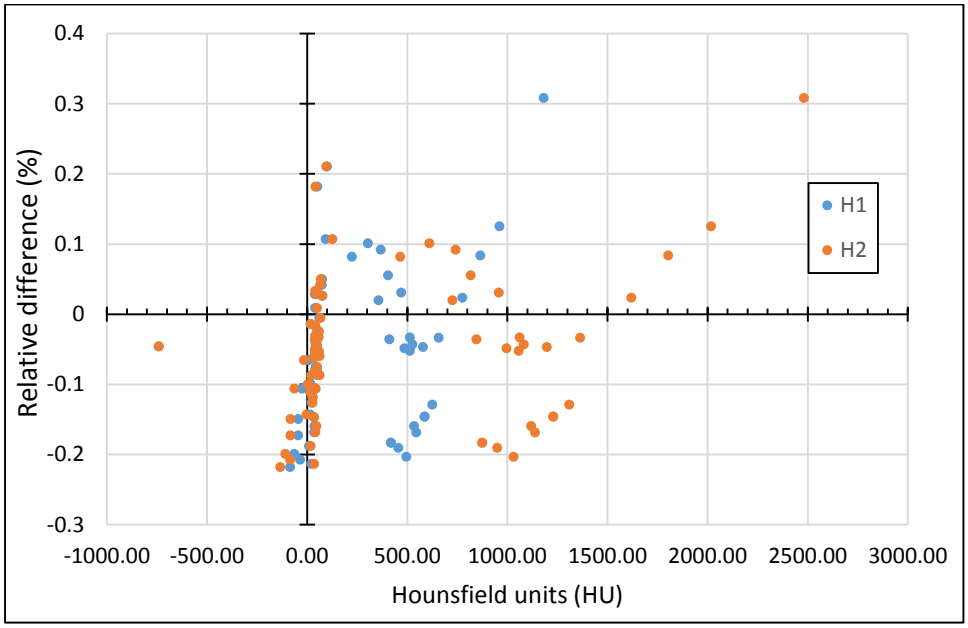

Figure 6, relative difference of RSP** vs. Hounsfield units, calibrated by KCl